Author Manuscript

Author Manuscript

Author Manuscript

Author Manuscript

HHS Public Access

Author manuscript

Radiat Phys Chem Oxf Engl 1993. Author manuscript; available in PMC 2021 November 01.

Published in final edited form as:

Radiat Phys Chem Oxf Engl 1993. 2020 November ; 176: . doi:10.1016/j.radphyschem.2020.109060.

Experimental validation of an analytical microdosimetric model based on Geant4-DNA simulations by using a silicon-based microdosimeter

A. Bertolet[1,4], **V. Grilj**[2], **C. Guardiola**[3], **A.D. Harken**[2], **M.A. Cortés-Giraldo**[4], **A. Baratto-Roldán**[4], **A. Carabe**[1]

[1]Department of Radiation Oncology, Hospital of The University of Pennsylvania, Philadelphia, PA, USA

[2]Radiological Research Accelerator Facility, Columbia University, Irvington, NY, USA

[3]Université Paris-Saclay, CNRS/IN2P3, IJCLab, 91405 Orsay, France; Université de Paris, IJCLab, 91405 Orsay France

[4]Department of Atomic, Molecular and Nuclear Physics, Universidad de Sevilla, Seville, Spain

Abstract

Purpose: To study the agreement between proton microdosimetric distributions measured with a silicon-based cylindrical microdosimeter and a previously published analytical microdosimetric model based on Geant4-DNA in-water Monte Carlo simulations for low energy proton beams.

Methods and material: Distributions for lineal energy (y) are measured for four proton monoenergetic beams with nominal energies from 2.0 MeV to 4.5 MeV, with a tissue equivalent proportional counter (TEPC) and a silicon-based microdosimeter. The actual energy for protons traversing the silicon-based microdosimeter is simulated with SRIM. Monoenergetic beams with these energies are simulated with Geant4-DNA code by simulating a water cylinder site of dimensions equal to those of the microdosimeter. The microdosimeter response is calibrated by using the distribution peaks obtained from the TEPC. Analytical calculations for $\bar{y}_F$ and $\bar{y}_D$ using our methodology based on spherical sites are also performed choosing the equivalent sphere to be checked against experimental results.

CRediT author statement

A. Bertolet: Conceptualization, Methodology, Software, Formal analysis, Writing – Original Draft, Visualization. **V. Grilj:** Methodology, Investigation, Validation, Resources. **C. Guardiola:** Investigation, Validation, Methodology, Software, Formal analysis, Writing – review & editing. **A. D. Harken:** Methodology, Investigation, Validation, Resources, Writing – Review & Editing. **M. A. Cortés-Giraldo:** Methodology, Software, Resources, Writing – Review & Editing, Supervision. A. **Baratto-Roldán**: Software, Validation. **A. Carabe:** Conceptualization, Validation, Investigation, Resources, Writing – Review & Editing, Supervision, Project administration, Funding acquisition.

Publisher's Disclaimer: This is a PDF file of an unedited manuscript that has been accepted for publication. As a service to our customers we are providing this early version of the manuscript. The manuscript will undergo copyediting, typesetting, and review of the resulting proof before it is published in its final form. Please note that during the production process errors may be discovered which could affect the content, and all legal disclaimers that apply to the journal pertain.

Declaration of interests

The authors declare that they have no known competing financial interests or personal relationships that could have appeared to influence the work reported in this paper.

Author Manuscript Author Manuscript Author Manuscript Author Manuscript

Results: Distributions for y at silicon are converted into tissue equivalent and compared to the Geant4-DNA simulated, yielding maximum deviations of 1.03% for $\bar{y}_F$ and 1.17% for $\bar{y}_D$. Our analytical method generates maximum deviations of 1.29% and 3.33%, respectively, with respect to experimental results.

Conclusion: Simulations in Geant4-DNA with ideal cylindrical sites in liquid water produce similar results to the measurements in an actual silicon-based cylindrical microdosimeter properly calibrated. The found agreement suggests the possibility to experimentally verify the calculated clinical $\bar{y}_D$ with our analytical method.

Keywords

microdosimetry; lineal energy; silicon detector; proton therapy; TEPC; Geant4-DNA

1. Introduction

Protons present increased values of linear energy transfer (LET) [1]–[6] which have been correlated with an increased biological effectiveness at the distal edge of clinical beams [7], [8]. For this reason, LET calculations capabilities are being introduced in treatment planning systems (TPS) for research purposes [9]–[11]. Additionally, in the case of further validation of that correlation, clinical treatments might need to consider LET besides dose to guide the treatment design. If that is the case, such LET distributions calculated by the TPS should be verified as part of the quality control program of the proton clinic. However, distributions of LET of the particles in a volume are challenging to be measured, so that measuring a closely related quantity to LET such as the lineal energy (y) becomes more convenient by employing microscopic-sized detectors, so-called microdosimeters. y is the microdosimetric equivalent to LET [12], [13], and is also correlated to biological effectiveness [14]–[21]. Lineal energy, unlike LET, is a stochastic quantity, meaning that distributions of occurrence are obtained for a given irradiation instead of deterministic values. Hence, y is capable of determining the volumetric patterns of energy deposition in microscopic structures [22], [23].

Lineal energy can be computed with dedicated microscopic Monte Carlo (MC) simulations [24]–[27], usually slower than analogous macroscopic MC simulations to compute LET. Nonetheless, it can be experimentally determined using tissue-equivalent proportional counters (TEPCs), which have been traditionally used [28]. These instruments, however, are filled with gas to simulate an equivalent microscopic site, which means that their actual size is macroscopic, producing some flaws that need to be corrected. To overcome this, mini-TEPC has been recently applied to measure more accurate microdosimetric distributions for proton beams [29], [30]. A different technology to address microdosimetric measurements is based on silicon detectors [31]–[34]. Unlike TEPC, new silicon-based 3D microdetectors do not need a gas supply, can reach microscopic size, and their ability to reproduce accurate microdosimetric spectra has been checked [35]–[37].

In previous works, we have developed a methodology able to compute 3D distributions of the dose-mean lineal energy within a patient [38]. In this work, we measure lineal energy distributions of low energy proton monoenergetic beams and compare the results with the

Author Manuscript Author Manuscript Author Manuscript Author Manuscript

mean values calculated analytically with our method, as well as MC-simulated distributions. Our goal is to validate our analytical calculation methodology [38], although restricted to the low proton energy region, to then assess its potential for experimental measurements in clinical scenarios.

2. Experimental methods

Microdosimetry deals with the interactions between radiation and matter at microscopic level, in which the stochastic nature of these interactions become prominent. In this context, the concept of microdosimetric site arises in order to define a region in which the energy deposited by radiation is accounted for. Thus, the energy imparted in a site, ε, is a stochastic quantity that varies from experiment to experiment or, in microdosimetric terms, from event to event, depending on the dimensions of the considered site. In the case of hadron beams, lineal energy (y), which represents the amount of energy imparted per unit chord length, might be a more meaningful quantity to characterize microdosimetric interactions. Lineal energy is defined as[12]

$$y = \frac{\varepsilon}{\bar{l}}, \tag{1}$$

where $\bar{l}$ is the mean chord length for the particle track within the site. This is a solved geometrical problem for sites of simple geometry [39], [40], with $\bar{l} = 2d/3$ for spheres of diameter d for isotropic radiation.

The resultant distribution of y, $f(y)$, obtained from the variable value of y per event, can be characterized by its mean value, $\bar{y}_F$. Nonetheless, this quantity disregards that high values of y, i.e., events with large energy imparted, are associated with harder damage to cells according to the theory of dual radiation action (TDRA) [41]. Therefore, the dose-weighted distribution of y, defined as $d(y) = yf(y)/\bar{y}_F$ represents a more convenient way to deal with lineal energy. Therefore, the average of $d(y)$, so-called dose-mean lineal energy $\bar{y}_D$ represents a single parameter that best characterizes the efficiency of a given radiation for producing biological damage.

2.1 Analytical models for microdosimetric calculations

A new analytical methodology to obtain mean values of microdosimetric distributions in clinical beams has been recently developed and published in Bertolet et al., 2019 [38]. In this approach, polyenergetic clinical beams, characterized by a spectral fluence $\phi_E(E)$, are decomposed into their spectral components. The mean energy imparted to a microscopic site for the polyenergetic beam $\bar{\varepsilon}$ can be expressed in terms of the mean energy imparted by monoenergetic beams of energy E, $\bar{\varepsilon}(E)$, by integrating as follows:

$$\bar{\varepsilon} = \frac{\int \phi_E(E)\bar{\varepsilon}(E)\mathrm{d}E}{\int \phi_E(E)\mathrm{d}E} \tag{2}$$

Author Manuscript Author Manuscript Author Manuscript Author Manuscript

Similarly, the variance of the energy imparted σ_ε^2 for a polyenergetic beam can be expressed in terms of the variances of energy imparted for monoenergetic beams $\sigma_\varepsilon^2(E)$, $\bar{\varepsilon}(E)$ and $\bar{\varepsilon}$ as [38]:

$$\sigma_\varepsilon^2 = \frac{\int \phi_E(E)\sigma_\varepsilon^2(E)\mathrm{d}E}{\int \phi_E(E)\mathrm{d}E} + \frac{\int \phi_E(E)(\bar{\varepsilon}(E)-\bar{\varepsilon})^2\mathrm{d}E}{\int \phi_E(E)\mathrm{d}E} \quad (3)$$

Therefore, by characterizing the values $\bar{\varepsilon}(E)$ and $\sigma_\varepsilon^2(E)$ for monoenergetic beams it is possible to obtain results applied to polyenergetic, i.e. clinical, beams. To do so, monoenergetic beams imparting energy to a spherical site were simulated using Geant4-DNA [42]–[45] with a code described in previous works [27], [38] and analytical functions for $\bar{\varepsilon}(E)$ and $\sigma_\varepsilon^2(E)$ were developed, among other microdosimetric quantities. This all allows for an analytical calculation of dose-averaged LET, $\bar{y}_F$ and $\bar{y}_D$ for both monoenergetic and clinical beams. Here, we validate both the Geant4-DNA code used and the analytical functions to model $\bar{\varepsilon}(E)$ and $\sigma_\varepsilon^2(E)$ for a set of experimentally available monoenergetic beams.

These calculations are based on spherical sites whereas our silicon-based microdosimeter is represented by a cylindrical site of 5.5 μm in length and 16 μm in diameter whose axis is oriented in parallel to the particle tracks. In order to assess whether it is possible to compare spherical-based results with experimental measurements with this device, we have considered the concept of *length-equivalent* sphere. As $\bar{y}_F$ is specific to the mean chord length, the hypothesis of equal $\bar{y}_F$ for equal site mean chord lengths is tested. This would imply that mean energies imparted to *length-equivalent* sites are the same. In the sphere case, the mean chord length for a site with diameter d is given by $\bar{l} = 2d/3$ so that we consider a sphere with 8.25 μm in diameter, which corresponds to a mean chord length of 5.5 μm. Nonetheless, the distribution of lineal energy $f(y)$ for that spherical site is expected to be wider than for its analogue cylindrical geometry due to the variability in the chord length happening in the first case but not in the second one, as particles traverse the microdosimeter parallel to its axis. This means that, even though $\bar{y}_F$ coincided for both geometries, $\bar{y}_D$ would be larger for the spherical case than for the cylindrical one, as $\bar{y}_D$ not only takes into account the mean energy imparted but also the variability in the distribution of energy imparted. According to Kellerer [46], [47], the impact on $\bar{y}_D$ of variability in the distribution of chord length in spherical sites can be approximated by a multiplicative factor given by the quotient between the mean and the weighted mean chord length for the spherical case. These means are defined as $\bar{l} = \int l f(l) dl$ and $\bar{l}_D = \int l^2 f(l) dl / \int l f(l) dl$, respectively, being the chord length distribution $f(l) = 2l/d^2$ for a spherical site with diameter d [39]. The mentioned quotient is then $\bar{l}/\bar{l}_D = 8/9$ for the spherical case. Thus, in this work, calculations of $\bar{y}_D$ carried out with our analytical model for a spherical site of 8.25 μm in diameter already contains the multiplicative factor 8/9 to be comparable to the results obtained with cylindrical sites.

Author Manuscript Author Manuscript Author Manuscript Author Manuscript

2.2 Experimental setup

Proton monoenergetic microbeams of a set of different nominal energies (2.0 MeV, 2.7 MeV, 3.4 MeV, 4.0 MeV and 4.5 MeV) were generated at the Radiological Research Accelerator Facility (RARAF) of the University of Columbia by a 5 MV Singletron accelerator. The experimental setup can be described as follows: vertical monoenergetic proton microbeams are magnetically collimated to several μm of diameter. Protons leave the vacuum system through a 2 μm-thick Mylar layer and a 2.89 μm-thick havar foil and traverse an air gap of 6 mm before reaching any device. There, a wheel is able to distribute the beam through three possible detectors independently (see Figure 1a), controlling the time of irradiation allocated to each one through the number of monitor counts. These three detectors are: (a) an ionization chamber in current mode that serves as a monitor chamber; (b) a solid-state detector (SSD) to measure the energy spectrum of the incoming beam; and (c) a TEPC in pulse mode, filled with gas to represent 6 μm tissue equivalency in a slab-like site that collects the charges produced by incoming particles, i.e., measures events of energy deposition, ε. Lineal energy at the TEPC can be then obtained, according to equation (1), as $y = \varepsilon/\bar{l} = \varepsilon/(6\,\mu\text{m})$. Note that, as the TEPC is a slab perpendicularly traversed by protons, its thickness, 6 μm, corresponds to the single chord length for any track, with in turn coincides with the mean chord length. Besides the 6 mm air gap, the beam needs to travel through 6 μm more of Mylar to arrive at the TEPC, which produces a certain loss on the kinetic energy of the beam.

Independently, the silicon-based 3D microdosimeter [32], [33], [35] was placed just at the exit of the 6 mm air gap (see Figure 1b) to measure the microdosimetric spectra of the nominal energies previously considered: 2.0 MeV, 2.7 MeV, 3.4 MeV and 4.5 MeV. This device represents a cylindrical microdosimetric site with dimensions of 5.5 μm in length and 16 μm in diameter. Since the pathway beams varies lightly from the TEPC to the microdosimeter, the actual kinetic energy for the particles conforming the beams is different at each detector. To overcome this, Monte Carlo simulations with the SRIM code [48] were performed to determine the real energy of the protons arriving at both TEPC and silicon-based 3D microdosimeter.

2.3 Calibration of the microdosimeter

The customized readout-electronic system provides a calibration curve between ADC channels and energy imparted, given by ε(keV)=0.253×ADC Channel+26.161. However, that calibration has been performed for thicker silicon detectors and, therefore, a calibration readjustment can be required for small sensitive volumes as that of the microdosimeter used herein. That calibration correction factor was performed by employing the measurements done with the TEPC. For this purpose, the ADC channel corresponding to the measured peak lineal energy, $\hat{y}_{TEPC}$, for each one of the employed beams was recorded so that four points (ADC channel, $\hat{y}_{TEPC}$) were obtained. Also, the TEPC measures energy deposition in tissue-equivalent gas while the microdosimeter does it in silicon, so the following transformation is required in order to obtain the equivalent TEPC peak lineal energy value in silicon. As we deal with monoenergetic beams, the peak lineal energy referred to silicon,

Author Manuscript Author Manuscript Author Manuscript Author Manuscript

$\hat{y}_{Si}$, can be obtained by applying directly the correction factor regarding the stopping power ratio of silicon to tissue [28]

$$\hat{y}_{Si} = \hat{y}_{TEPC} \times \frac{S_{Si}(E)}{S_{TE}(E)}, \quad (4)$$

where E is the energy of the monoenergetic microbeam within the microdosimeter, and $S_{Si}(E)$ and $S_{TE}(E)$ are, respectively, the stopping power of silicon and tissue for that energy, which we obtained from the PSTAR database of the National Institute of Standards and Technology (NIST). This simple transformation when mono-energetic beams are used for the calibration, as long as the stopping power ratio can be considered relatively constant along the active volume of the detector. Note that the same process for polyenergetic beams would require the knowledge of the energetic spectrum, which could be obtained by using telescopic detection systems [49]. δ-ray equilibrium was assumed to be immediately achieved in both detectors as secondary electrons released in ionization collisions of protons with the energies considered in this work have ranges much lower than the longitudinal dimension of both detectors.

As mentioned above, the path that beams have to travel to reach the TEPC or the microdosimeter are different, so that the actual energy of the particles arriving to them from a beam is different. This means that a direct relation between peak energies as in equation (4) is not possible, since E changes from one detector to the other. Our approach then to obtain the values $\hat{y}_{Si}$ for the calibration correction was to use a cubic-spline interpolation of the corresponding value $\hat{y}_{TEPC}$ between the actual energies registered at the TEPC and then use equation (4). To obtain the peak energies $\hat{\varepsilon}_{Si}$ to finally perform the calibration, according to equation (1), lineal energy is multiplied by the mean chord length in the microdosimeter, which is a cylinder of 5.5 μm in length oriented parallel to the beam axis, so that $\bar{l} = 5.5$ μm. Note that the concept of mean chord length is used here to keep consistency with the spherical case, although a single path length is obtained for this cylindrical geometry.

2.4 Converting silicon readouts into tissue-equivalent

Raw measurements from the calibrated microdosimeter provide $f(\varepsilon_{si})$, i.e. the distribution of energy imparted in the silicon site, ε_{si}. To obtain the corresponding distribution of lineal energy, $f(y_{si})$, it is necessary to divide ε_{si} by the mean chord length in the site, $\bar{l}$. However, the non-tissue equivalence of the silicon of which the cylindrical site is made needs to be corrected by $y_{TE} = y_{si} \times S_{TE}(E)/S_{Si}(E)$ in a similar way as done in equation (4).

2.5 Calculating $\bar{y}_F$ and $\bar{y}_D$

Finally, the values for the averages of frequency and dose-weighted distributions for y can be calculated from the measured distribution referred to tissue-equivalent as follows:

$$\bar{y}_F = \frac{\sum y f(y)}{\sum f(y)} \quad (5)$$

Author Manuscript Author Manuscript Author Manuscript Author Manuscript

and

$$\bar{y}_D = \frac{\sum y\, d(y)}{\sum d(y)} = \frac{\sum y^2 f(y)}{\sum y\, f(y)}. \quad (6)$$

To estimate the uncertainties for these two experimental results, we assume that the effect of the uncertainty in the TEPC peak $\hat{y}_{TEPC}$ is smaller than the uncertainty provided by the calibration curve for the energy deposited in silicon. This uncertainty can be estimated by means of the root mean square of the residuals between the data points from the TEPC and the fitted function. Then, it can be propagated according to equation (1) and added to the intrinsic uncertainty for the expressions in equations (5) and (6) assuming a Poisson distribution for $f(y)$.

2.6 Geant4-DNA simulations

The same monoenergetic proton beams, with the actual energy arriving at the microdosimeter. were simulated in liquid water and converted to tissue-equivalent in a similar way as equation (4) shows in order to check the validity of the Geant4-DNA code employed to develop our analytical model. Instead of spherical sites, we used a cylindrical site with dimensions of 5.5 μm in length and 16 μm as basis diameter to match the site with the employed microdosimeter. Tracks for primary protons were originated from a point source to penetrate a liquid water box with an inner box to score energy deposition inside, extended with margins -upstream, downstream and lateral- equal to the maximum range of secondary electrons for each beam according to Tabata's formula [50]. The cylinder axis is oriented parallel to the beam axis, as it happens in the experiment. The position for the cylinder was sorted uniformly in the inner box for each primary proton track, i.e., for each event to reproduce the situation in which the cylinder is irradiated by a uniform proton beam. The default physics list constructor of Geant4-DNA [45] was employed, which simulates protons and electrons down to 1 keV and 7.4 eV, respectively. Simulations of track structure included secondary electrons in the entire liquid water box. Cross sections for ionization and excitation processes were calculated using the First Born Approximation and the Emfietzoglou dielectric model [43], [45], [51]. Geant4-DNA provides the user with various options for physics lists which incorporate different cross-section models and data relevant for electron transport. However, according to dose-point kernels calculated for monoenergetic electrons by Kyriakou et al. [52], it seems that their influence would become noticeable for sensitive volumes of the order of tens of nanometers. Further details on the Geant4-DNA application can be found in previous works [27], [38], [53]. Uncertainties for $\bar{y}_F$ and $\bar{y}_D$ are calculated following the procedure exposed in the Appendix of Bertolet et al. 2019 [27].

3. Results

Table 1 shows the results obtained from the SRIM simulations to determine the beam energy arriving at each considered detector. Beam energies are higher at the entrance of the microdosimeter than the TEPC entrance as the thickness particles need to go through is

Author Manuscript Author Manuscript Author Manuscript Author Manuscript

thinner in the former. The measured values for the peak of lineal energy at the TEPC, $\hat{y}_{TEPC}$, for all these beams are also shown.

Figure 2 shows the obtained calibration between ADC channels and energy imparted in silicon converted from measured peak lineal energies at the TEPC as described in section 'Calibration of the microdosimeter'. The following relation is obtained by fitting a straight line to the measured data:

$$\varepsilon\,(\mathrm{keV}) = 0.456 \times C + 13.55, \tag{7}$$

where C represents the ADC channel. The goodness of the fit can be assessed through the R^2 value, that yields the value 0.997.

Measured distributions with the calibrated microdosimeter compared to the obtained from simulations with cylindrical sites in Geant4-DNA are shown in Figure 3 for beams with energies equal to the obtained in Table 1 to arrive at the microdosimeter. The distributions $yd(y)$ is represented in logarithmic scale for the four beam energies considered at the entrance of the microdosimeter.

Fig. 4 shows the results for $\bar{y}_F$ and $\bar{y}_D$ obtained from distributions shown in Fig. 3, as well as their analytically calculated values for a spherical site of 8.25 μm in diameter according to the subsection 'Analytical calculations'.

Table 2 shows the maximum difference and the root mean square for the residuals obtained between the three set of data points. Maximum relative differences are also shown. The base of the percentage difference is always the experimental value, except when comparing the analytical and the simulation, in which case, the latter is used.

4. Discussion

The calibration readjustment process is based on the assumption that the employed beams are monoenergetic and the stopping power ratio for the protons does not vary considerably along the portion of their track inside the microdetectors. This can be evaluated by calculating the residual range of the protons at the exit of the detectors and the corresponding stopping power both in water and in silicon. In the worst case (1.55 MeV), the variation on the stopping power ratio is below 2%.

The distributions shown in Fig. 3 should be analyzed in terms of two of their features: the position of the peak and the spread around that peak. For the experimental distribution, the former can be attributable to the TEPC measurements, since those data are carried through the calibration function shown in Fig. 2, plus the error introduced by the calibration process itself. The two mentioned features can be associated, respectively, to $\bar{y}_F$ and $\bar{y}_D$, given that weighted averages are a combined expression of the mean and the variance of a distribution as deductible from equation (6). Even though $\bar{y}_F$ depends on the mean and not on the peak of the distribution $f(y)$, at least at a first approximation, both parameters are correlated.

Author Manuscript Author Manuscript Author Manuscript Author Manuscript

Looking at Fig. 3, distributions from the compounded process of microdosimeter readout, calibration and transformation into tissue-equivalent results seem to match the position on the energy imparted range of the distributions obtained from our Geant4-DNA application. It should be noted that these simulations are carried out in an ideal setup all made of liquid water, meaning no interface between materials occurs, with protons perfectly aligned with the cylinder axis. Even then, the ability of our application to reproduce the peak position of the distributions looks valid against the microdosimeter. Furthermore, not only the positions but also the shapes of the depicted distributions tend to reasonably coincide, except for the visible tail at the low energy part for the experimental distribution. The origin for this tail may consist of the scattered protons passing through the 2 μm mylar inside the vacuum pipe and exit window and air gap before reaching the microdosimeter. Scattering in the exit aperture may also contribute to the lower energy tail. Even if those protons had not lost much of their energy, their track will bend, so that they do not travel parallel to the cylinder axis. In this case, the chord length distribution deviates from the expected one. These short chord-length events mean protons undergoing fewer collisions in the detector and, consequently, depositing less energy. Those tails do not seem to affect the averages $\bar{y}_F$ and $\bar{y}_D$ much, though, and therefore there is probably no need to incorporate those events to the ideal G4-DNA simulations.

The higher uncertainty for $\bar{y}_D$ is explained by the fact that it depends not only on the mean value of $f(y)$ (as $\bar{y}_F$ does too), but also on its variance, which, in turn, carries an extra amount of uncertainty. They both are, essentially, reduced to the error coming from the calibration process, since their statistical uncertainties decrease with the number of events registered in the detector, i.e., with the exposure time. Now, the differences between measured and simulated $\bar{y}_F$ and $\bar{y}_D$ are within the uncertainties visible in Fig. 4.

The dashed curve in Fig. 4 is the result of our analytical model for these monoenergetic beams as particular cases. Even though the agreement with the experimental results is poorer than for the dedicated cylindrical simulations, both averages for y yield reasonable differences of <4%, as seen in Table 2. Further, the analytical calculations here employed used models for a spherical site with diameter of 8.25 μm, which are obtained from interpolation between the sites dimensions used to create the models [38]: 1 μm, 5 μm and 10 μm. This interpolation introduces a larger uncertainty on the result. The validity of the shown agreement is limited to low energies in this work and further investigation is needed to extend it beyond 5 MeV. This method potentially may be applicable to other clinically relevant energies as long as the physics models in Geant4-DNA remains accurate, since the code employed to obtain microdosimetric data is the same. However, Geant4-DNA is currently limited to 100 MeV, although above this energy a macroscopic description of the energy deposition may be sufficient due to the relatively long range for protons at such energies.

The silicon microdosimeter's response can be considered as independent of the beam energy, as shown in works where measurements were taken at different positions of the depth-dose curve, i.e. different energy spectra [33], [34], [36]. Therefore, the measurement of $\bar{y}_F$ and $\bar{y}_D$ referred to silicon should be accurate for the whole clinical energy range,

Author Manuscript Author Manuscript Author Manuscript Author Manuscript

keeping in mind that its transformation into tissue-equivalent distributions, according to equation (4), depends on the energy spectrum. As shown in equations (2) and (3), energy-dependent functions can be integrated over a pre-calculated spectrum [54] to calculate microdosimetric quantities for polyenergetic beams. This can be used for direct comparisons between values calculated for clinical beams in a treatment planning system (TPS) in which that pre-calculated spectra are incorporated, and experimental measurements with silicon-based detectors for clinical beams. In other words, both analytical calculation and experimental measurements are feasible even for clinically relevant energies and polyenergetic beams. Nonetheless, the agreement between them needs to be corroborated in further works.

5. Conclusions

Silicon-based microdosimeter can be employed to characterize microdosimetric distributions of lineal energy. Here, we present a method to calibrate it by employing monoenergetic proton beams along a TEPC serving as primary reference. On the other hand, Geant4-DNA simulations for ideal cylindrical sites in liquid water can be performed to emulate the measurements. Since an analytical methodology for TPS calculations is built based on those simulations, this correspondence allows for eventual correlation between calculated clinical $\bar{y}_D$ distributions and experimental measurements.

Acknowledgements and Disclosure of Conflicts of Interest

A. Bertolet and A. Carabe are supported by Varian Medical Systems, Palo Alto, California. V. Grilj and A. Harken are supported by the Radiological Research Accelerator Facility through the National Institute of Biomedical Imaging and Bioengineering (NIBIB) grant 5P41 EB002033. C. Guardiola has received funding from the European Union's Horizon 2020 research and innovation program under the Marie Sklodowska-Curie grant agreement No 745109. C. Guardiola, M. A. Cortés-Giraldo and A. Baratto-Roldán have not any relation with whatever private funding source. M. A. Cortés-Giraldo has been funded by the Spanish Government under Grant No. RTI2018-098117-B-C21. Baratto-Roldán is funded by the European Union's Horizon 2020 research and innovation program under the Marie Sklodowska-Curie Grant No. 675265, OMA-Optimization of Medical Accelerators. The Monte Carlo simulations were carried out at the FIS-ATOM computing cluster hosted at CICA (Seville, Spain).

References

[1]. Chen Y and Ahmad S, "Empirical model estimation of relative biological effectiveness for proton beam therapy," Radiat. Prot. Dosimetry, vol. 149, no. 2, pp. 116–123, 2012. [PubMed: 21593038]

[2]. Barendsen GW, "The Relationships between RBE and LET for Different Types of Lethal Damage in Mammalian Cells: Biophysical and Molecular Mechanisms," Radiat. Res, vol. 139, no. 3, pp. 257–270, 1994. [PubMed: 8073108]

[3]. Kuperman VY, "Cell kill by megavoltage protons with high LET," Phys. Med. Biol, vol. 61, no. 14, pp. 5183–5197, 2016. [PubMed: 27351166]

[4]. McMahon SJ, Paganetti H, and Prise KM, "LET-weighted doses effectively reduce biological variability in proton radiotherapy planning," Phys. Med. Biol, vol. 63, p. 225009, 2018.

[5]. Chaudhary P et al., "Relative Biological Effectiveness Variation Along Monoenergetic and Modulated Bragg Peaks of a 62-MeV Therapeutic Proton Beam: A Preclinical Assessment," Int. J. Radiat. Oncol, vol. 90, no. 1, pp. 27–35, 9 2014.

[6]. Britten RA et al., "Variations in the RBE for Cell Killing Along the Depth-Dose Profile of a Modulated Proton Therapy Beam," Radiat. Res, vol. 179, no. 1, pp. 21–28, 1 2013. [PubMed: 23148508]

Author Manuscript Author Manuscript Author Manuscript Author Manuscript

[7]. Wouters BG et al., "Radiobiological Intercomparison of the 160 MeV and 230 MeV Proton Therapy Beams at the Harvard Cyclotron Laboratory and at Massachusetts General Hospital," Radiat. Res, vol. 183, no. 2, p. 174, 2015. [PubMed: 25587741]

[8]. Peeler CR et al., "Clinical evidence of variable proton biological effectiveness in pediatric patients treated for ependymoma," Radiother. Oncol, vol. 121, no. 3, pp. 395–401, 12 2016. [PubMed: 27863964]

[9]. Giantsoudi D, Grassberger C, Craft D, Niemierko A, Trofimov A, and Paganetti H, "Linear energy transfer-guided optimization in intensity modulated proton therapy: Feasibility study and clinical potential," Int. J. Radiat. Oncol. Biol. Phys, vol. 87, no. 1, pp. 216–222, 2013. [PubMed: 23790771]

[10]. Fager M et al., "Linear Energy Transfer Painting With Proton Therapy: A Means of Reducing Radiation Doses With Equivalent Clinical Effectiveness," Int. J. Radiat. Oncol, vol. 91, no. 5, pp. 1057–1064, 4 2015.

[11]. Sánchez-Parcerisa D, López-Aguirre M, Dolcet Llerena A, Udías JM, Llerena AD, and Ud M, "MultiRBE: Treatment planning for protons with selective radiobiological effectiveness," Med. Phys, vol. 46, no. 9, pp. 4276–4284, 2019. [PubMed: 31310683]

[12]. ICRU, "Report 36. Microdosimetry," 1983.

[13]. Kellerer AM and Chmelevsky D, "Concepts of microdosimetry - I. Quantities," Radiat. Environ. Biophys, vol. 12, no. 2, pp. 61–69, 1975. [PubMed: 1178822]

[14]. Hawkins RB, "A microdosimetric-kinetic model of cell death from exposure to ionizing radiation of any LET, with experimental and clinical applications," Int. J. Radiat. Biol, vol. 69, no. 6, pp. 739–755, 1996. [PubMed: 8691026]

[15]. Hawkins RB, "A Microdosimetric-Kinetic Model for the Effect of Non-Poisson Distribution of Lethal Lesions on the Variation of RBE with LET," Radiat. Res, vol. 160, no. 1, pp. 61–69, 2003. [PubMed: 12816524]

[16]. Sato T, Watanabe R, Sihver L, and Niita K, "Applications of the microdosimetric function implemented in the macroscopic particle transport simulation code PHITS," Int. J. Radiat. Biol, vol. 88, no. 1–2, pp. 143–150, 1 2012. [PubMed: 21823823]

[17]. Takada K et al., "Validation of the physical and RBE-weighted dose estimator based on PHITS coupled with a microdosimetric kinetic model for proton therapy," J. Radiat. Res, vol. 59, no. 1, pp. 91–99, 1 2018. [PubMed: 29087492]

[18]. Scholz M, "Dose Response of Biological Systems to Low-and High-LET Radiation," in Microdosimetric Response of Physical and Biological Systems to Low-and High-LET Radiations, Horowitz Y, Ed. 2006, pp. 1–73.

[19]. Stewart RD, Yu VK, Georgakilas AG, Koumenis C, Park JH, and Carlson DJ, "Effects of Radiation Quality and Oxygen on Clustered DNA Lesions and Cell Death," Radiat. Res, vol. 176, no. 5, pp. 587–602, 2011. [PubMed: 21823972]

[20]. Lindborg L, Hultqvist M, Carlsson Tedgren Å, and Nikjoo H, "Lineal energy and radiation quality in radiation therapy: Model calculations and comparison with experiment," Phys. Med. Biol, vol. 58, no. 10, pp. 3089–3105, 2013. [PubMed: 23594445]

[21]. Nikjoo H, Emfietzoglou D, Liamsuwan T, Taleei R, Liljequist D, and Uehara S, "Radiation track, DNA damage and response - A review," Reports Prog. Phys, vol. 79, no. 11, 2016.

[22]. Chmelevsky D and Kellerer AM, "Computation of microdosimetric distributions for small sites," Radiat. Environ. Biophys, vol. 14, no. 2, pp. 123–136, 1977. [PubMed: 897064]

[23]. Grassberger C and Paganetti H, "Elevated LET components in clinical proton beams," Phys. Med. Biol, vol. 56, no. 20, pp. 6677–6691, 2011. [PubMed: 21965268]

[24]. Brenner DJ and Zaider M, "The Application of Track Calculations to Radiobiology: II. Calculations of Microdosimetric Quantities," Radiat. Res, vol. 98, no. 1, p. pp.14–25, 1984. [PubMed: 6326181]

[25]. Villegas F, Tilly N, and Ahnesjö A, "Target Size Variation in Microdosimetric Distributions and its Impact on the Linear-Quadratic Parameterization of Cell Survival," Radiat. Res, vol. 190, no. 5, pp. 504–512, 2018. [PubMed: 30106343]

Author Manuscript Author Manuscript Author Manuscript Author Manuscript

[26]. Newpower M et al., “Using the Proton Energy Spectrum and Microdosimetry To Model Proton Relative Biological Effectiveness,” Int. J. Radiat. Oncol. • Biol. • Phys, vol. 104, no. 2, pp. 316–324, 2019. [PubMed: 30731186]

[27]. Bertolet A, Baratto-Roldán A, Barbieri S, Baiocco G, Carabe A, and Cortés-Giraldo MA, “Dose-averaged LET calculation for proton track segments using microdosimetric Monte Carlo simulations,” Med. Phys, vol. 46, no. 9, pp. 4184–4192, 7 2019. [PubMed: 31169910]

[28]. Lindborg L and Waker A, Microdosimetry. Experimental Methods and Applications CRC Press, 2017.

[29]. Conte V et al., “Microdosimetry at the CATANA 62-MeV proton beam with a sealed miniaturized TEPC,” Phys. Medica, vol. 64, no. June, pp. 114–122, 2019.

[30]. Mazzucconi D et al., “Nano-microdosimetric investigation at the therapeutic proton irradiation line of CATANA,” Radiat. Meas, vol. 123, no. February, pp. 26–33, 2019.

[31]. Rosenfeld AB et al., “A new silicon detector for microdosimetry applications in proton therapy,” IEEE Trans. Nucl. Sci, vol. 47, no. 4 PART 1, pp. 1386–1394, 2000.

[32]. Guardiola C et al., “Silicon-based three-dimensional microstructures for radiation dosimetry in hadrontherapy,” Appl. Phys. Lett, vol. 107, no. 2, pp. 1–6, 2015.

[33]. Guardiola C et al., “Preliminary microdosimetric measurements with ultra-thin 3D silicon detectors of a 62MeV proton beam,” J. Instrum, vol. 10, no. 1, p. P01008, 2015.

[34]. Anderson SE et al., “Microdosimetric measurements of a clinical proton beam with micrometer-sized solid-state detector,” Med. Phys, vol. 44, no. 11, pp. 6029–6037, 2017. [PubMed: 28905399]

[35]. Gómez F et al., “Measurement of carbon ion microdosimetric distributions with ultrathin 3D silicon diodes,” Phys. Med. Biol, vol. 61, no. 11, pp. 4036–4047, 2016. [PubMed: 27163881]

[36]. Prieto-pena J et al., “Microdosimetric spectra measurements on a clinical carbon beam at nominal therapeutic fluence rate with silicon cylindrical microdosimeters,” IEEE Trans. Nucl. Sci, vol. 66, no. 7, pp. 1–1, 2019.

[37]. Bolst D et al., “Correction factors to convert microdosimetry measurements in silicon to tissue in 12C ion therapy,” Phys. Med. Biol, vol. 62, no. 6, pp. 2055–2069, 2017. [PubMed: 28151733]

[38]. Bertolet A, Baratto-Roldán A, Cortés-Giraldo MA, and Carabe-Fernandez A, “Segment-averaged LET concept and analytical calculation from microdosimetric quantities in proton radiation therapy,” Med. Phys, vol. 46, no. 9, pp. 4204–4214, 2019. [PubMed: 31228264]

[39]. Kellerer AM, “Chord-Length Distributions and Related Quantities for Spheroids,” Radiat. Res, vol. 98, no. 1, pp. 425–437, 1984.

[40]. Magrin G, “A method to convert spectra from slab microdosimeters in therapeutic ion-beams to the spectra referring to microdosimeters of different shapes and material,” Phys. Med. Biol, vol. 63, no. 21, 2018.

[41]. Kellerer AM and Rossi HH, “The Theory of Dual Radiation Action,” in Current Topics in Radiation Research. Volume VIII, Ebert M and Howard A, Eds. Manchester, U.K.: American Elsevier Publishing Company, 1974, pp. 85–156.

[42]. Incerti S et al., “The Geant4-DNA project,” Int. J. Model. Simulation, Sci. Comput, vol. 1, no. 2, p. 157, 2010.

[43]. Incerti S et al., “Comparison of GEANT4 very low energy cross section models with experimental data in water,” Med. Phys, vol. 37, no. 9, pp. 4692–4708, 2010. [PubMed: 20964188]

[44]. Bernal MA et al., “Track structure modeling in liquid water: A review of the Geant4-DNA very low energy extension of the Geant4 Monte Carlo simulation toolkit,” Phys. Medica, vol. 31, no. 8, pp. 861–874, 12 2015.

[45]. Incerti S et al., “Geant4-DNA example applications for track structure simulations in liquid water: A report from the Geant4-DNA Project,” Med. Phys, vol. 45, no. 8, pp. e722–e739, 2018.

[46]. Kellerer AM, “Analysis of Patterns of Energy Deposition,” in Second Symposium on Microdosimetry, 1970, pp. 107–136.

[47]. Kellerer AM, “Fundamentals of microdosimetry,” in The Dosimetry of Ionization Radiation. *Volume* I, Kase KR, Bjarngard BE, and Attix FH, Eds. Orlando, FL: Academic Press, Inc., 1985, pp. 77–162.

Author Manuscript Author Manuscript Author Manuscript Author Manuscript

[48]. Ziegler JF, Ziegler MD, and Biersack JP, “SRIM – The stopping and range of ions in matter (2010),” Nucl. Inst. Methods Phys. Res. B, vol. 268, no. 11–12, pp. 1818–1823, 2010.

[49]. Agosteo S et al., “Study of a monolithic silicon telescope for solid state microdosimetry: Response to a 100 MeV proton beam,” Radiat. Meas, vol. 46, no. 12, pp. 1529–1533, 2011.

[50]. Tabata T, Ito R, and Okabe S, “Generalized semiempirical equations for the extrapolated range of electrons,” Nucl. Instruments Methods, vol. 103, pp. 85–91, 1972.

[51]. Emfietzoglou D, “Inelastic cross-sections for electron transport in liquid water: A comparison of dielectric models,” Radiat. Phys. Chem, vol. 66, no. 6, pp. 373–385, 2003.

[52]. Kyriakou I, Šefl M, Nourry V, and Incerti S, “The impact of new Geant4-DNA cross section models on electron track structure simulations in liquid water,” J. Appl. Phys, vol. 119, no. 19, 2016.

[53]. Baratto-Roldán A, Kimstrand P, Perales Á, Carabe A, and Cortés-Giraldo MA, “Abstract ID: 196 Relation between dose average linear energy transfer and dose mean lineal energy calculated for proton therapy beams off axis: A study with the Geant4 toolkit.,” Phys. Medica, vol. 42, no. 2017, pp. 42–43, 2017.

[54]. Bertolet A, Cortés-Giraldo MA, Souris K, and Carabe A, “A kernel-based algorithm for the spectral fluence of clinical proton beams to calculate dose-averaged LET and other dosimetric quantities of interest,” Med. Phys, pp. 1–11, 2020. [PubMed: 31663612]

Author Manuscript Author Manuscript Author Manuscript Author Manuscript

Highlights

- Validation of analytical microdosimetric models for protons of low energy
- Silicon-based microdosimeter is calibrated and employed for experimental data
- Distributions and averages of lineal energy are compared
- We found agreement among experiments, Geant4-DNA and analytical results

Author Manuscript Author Manuscript Author Manuscript Author Manuscript

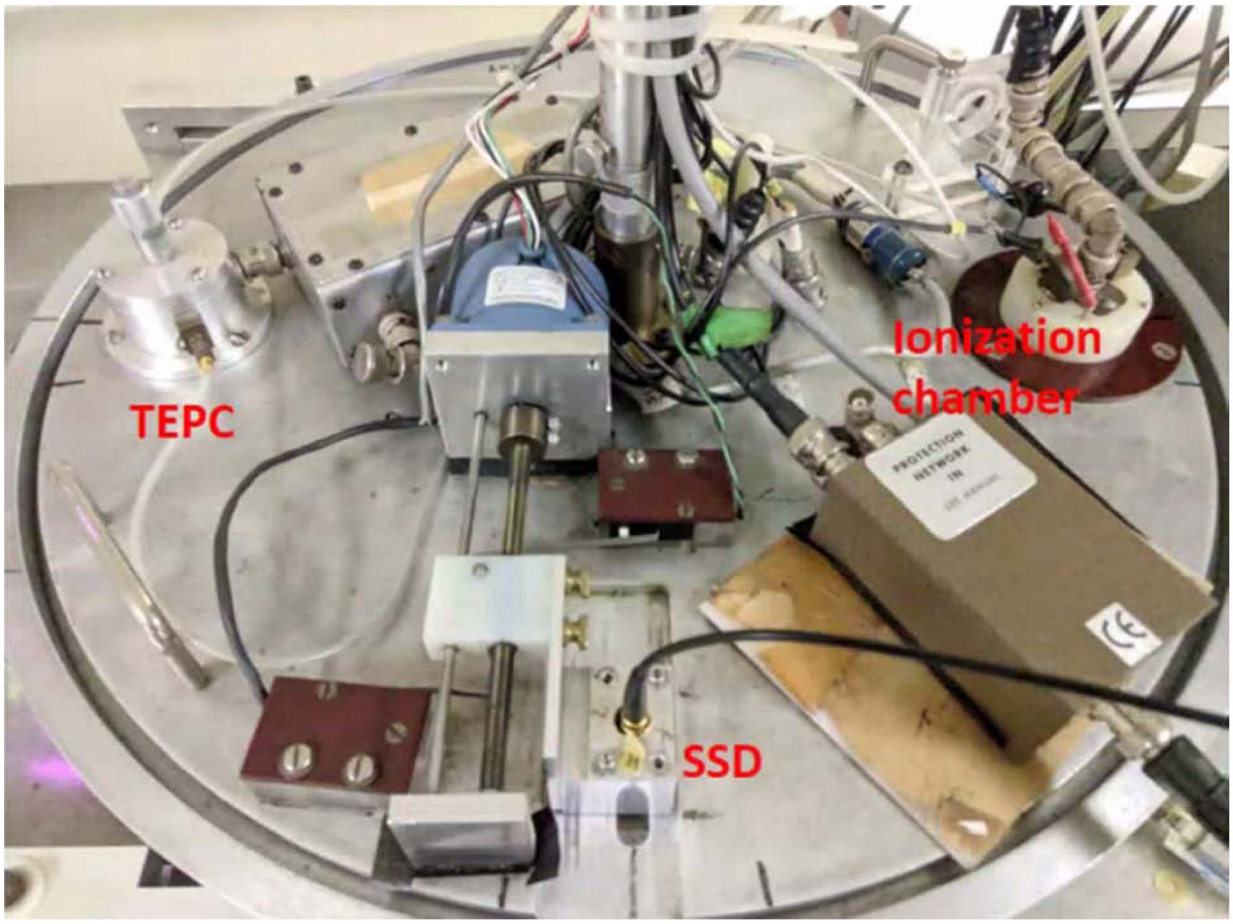

Author Manuscript Author Manuscript Author Manuscript Author Manuscript

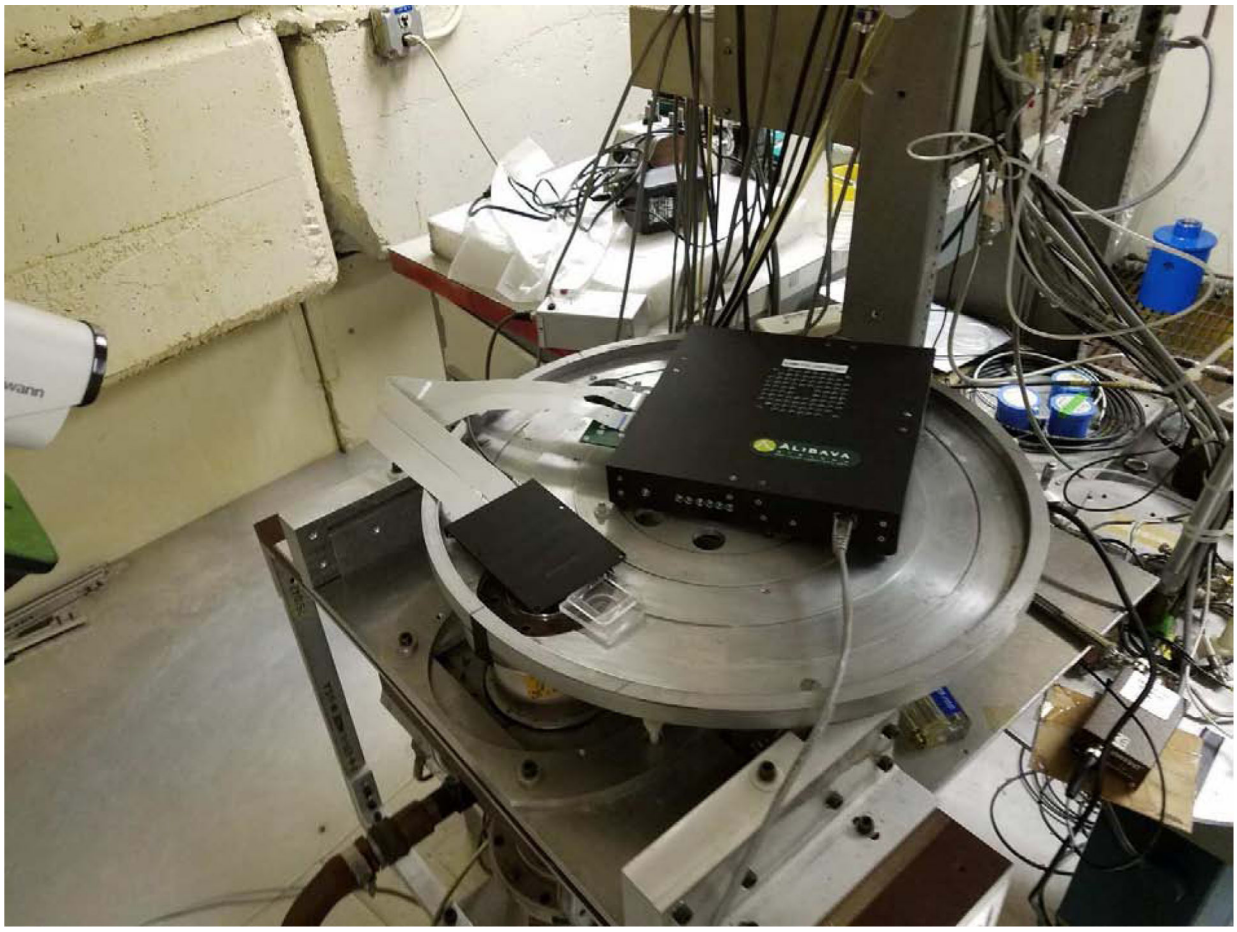

Figure 1.
Pictures of the experimental setup for: **(a)** TEPC measurements and **(b)** silicon-based 3D microdosimeter measurements.

Author Manuscript Author Manuscript Author Manuscript Author Manuscript

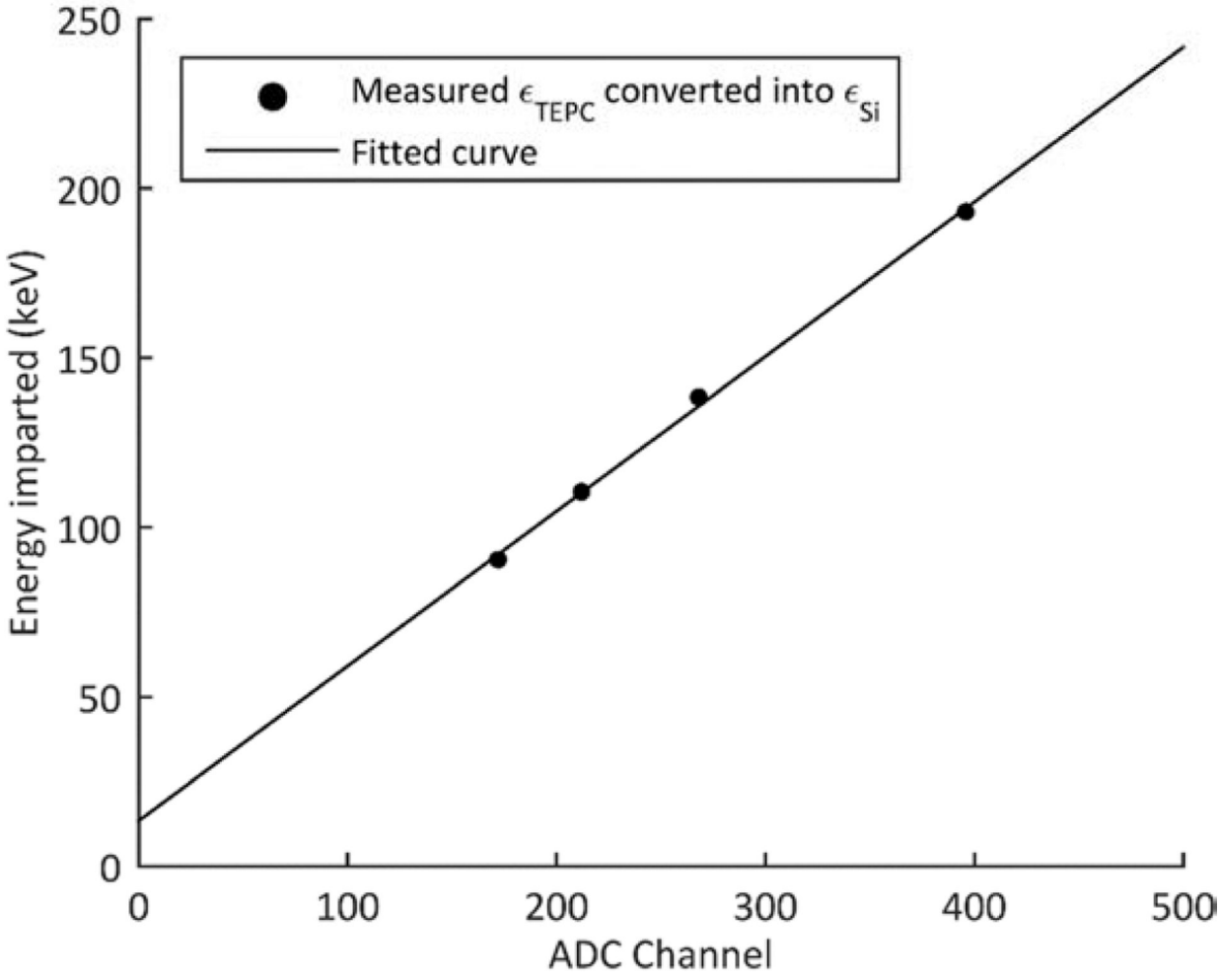

Figure 2.

Calibration curve obtained for the relation between ADC channel and energy imparted into the silicon-based microdosimeter. The resulting fit yields the relation ε, (keV) = 0.456×C +13.55. with R^2 = 997.

Author Manuscript Author Manuscript Author Manuscript Author Manuscript

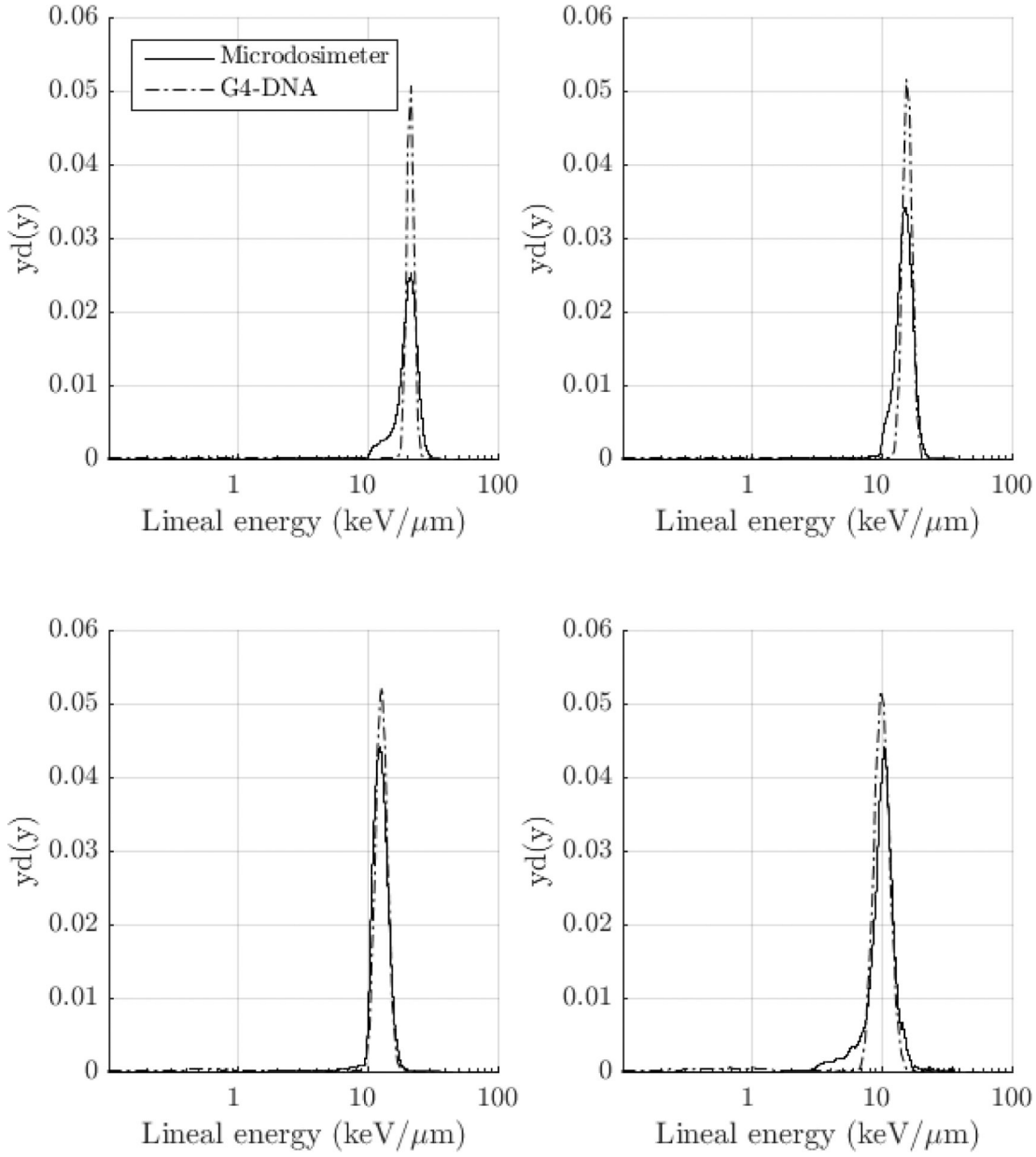

Figure 3.

Microdosimetric spectra in tissue represented as in logarithmic scale for *yd*(*y*) microdosimeter measurements and simulations with Geant4-DNA for beams with energies: (a) left upper: 1.55 MeV; (b) right upper: 2.30 MeV; (c) left bottom: 3.01 MeV; and (d) right bottom: 4.12 MeV. Values express the mean energy at entrance in the sensitive volume. Measured spectra in silicon with the microdosimeter are transformed into tissue by multiplying by the stopping power ratio of these media.

Author Manuscript Author Manuscript Author Manuscript Author Manuscript

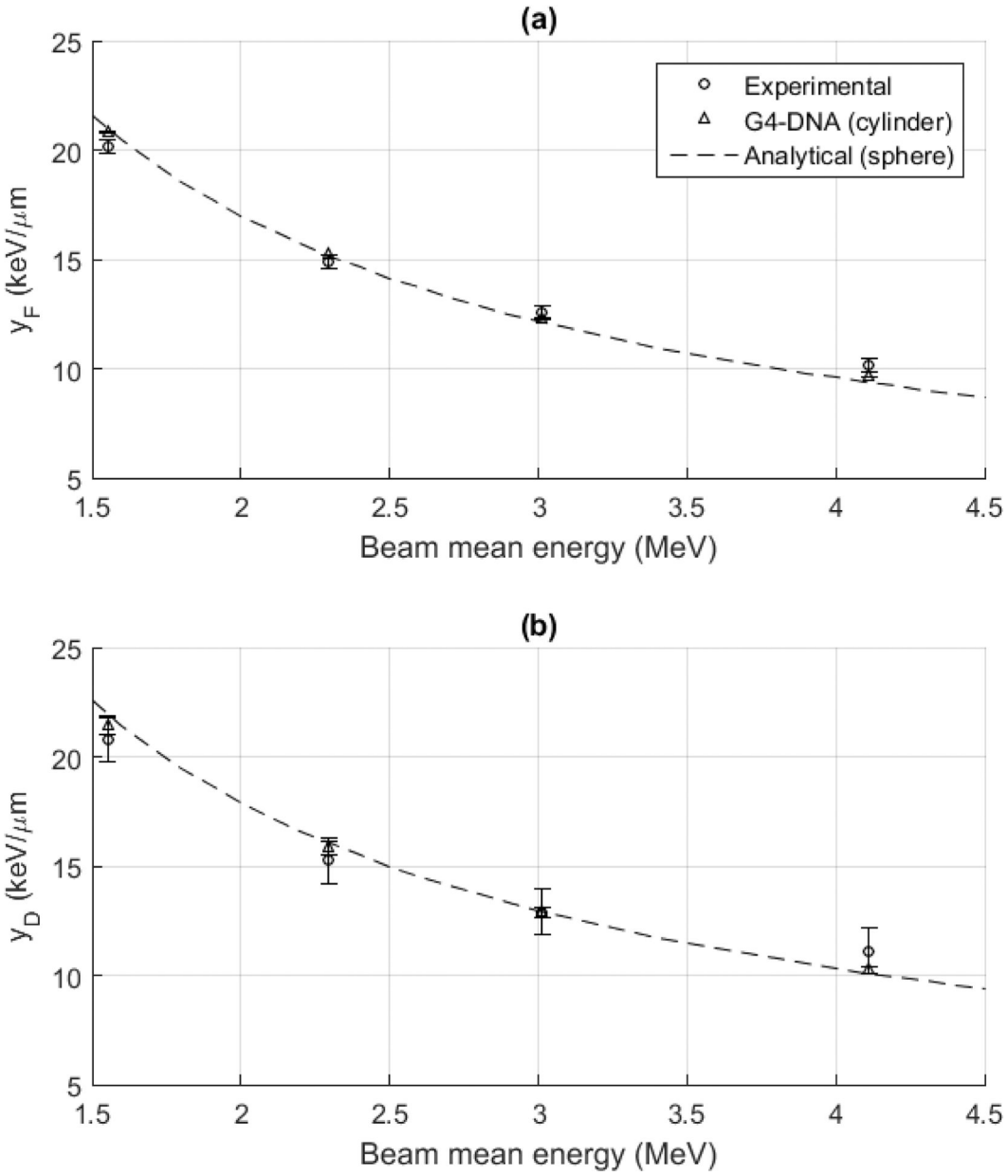

Figure 4.

Results for: (a) $\bar{y}_F$; and (b) $\bar{y}_D$, obtained experimentally from the $f(y)$ distributions measured with the silicon based microdosimeter and simulated with Geant4-DNA for beam mean energies equal to 1.55 MeV, 2.30 MeV, 3.01 MeV and 4.12 MeV at the entrance of the sensitive volume. The dashed curves represent the analytical calculation for $\bar{y}_F$ and $\bar{y}_D$ developed by Bertolet et al.[38] based on a microdosimetric spherical site of 8.25 μm in diameter, which is expected to be equivalent to a cylinder with 5.5 μm in length. Analytical calculations for $\bar{y}_D$ already carry a multiplicative factor equal to 8/9 to compensate the larger variance in a spherical site with respect to a cylindrical one. Uncertainties of the measurements and G4-DNA simulations (1σ) are shown with error bars.

Author Manuscript

Author Manuscript

Author Manuscript

Author Manuscript

Table 1.

Mean energies at the entrance of the TEPC and the microdosimeter for each nominal energy according to simulations with the MC code SRIM. The last column shows the peak in terms of lineal energy $\hat{y}_{TEPC}$ measured at the TEPC.

Nominal Energy (MeV)	Mean energy at TEPC (MeV)	Mean energy at microdosimeter (MeV)	Lineal energy peak at TEPC $\hat{y}_{TEPC}$ (keV/μm)
2.00	1.39	1.55	21.73
2.70	2.18	2.30	15.22
3.40	2.92	3.01	11.98
4.50	4.04	4.12	9.67

Author Manuscript

Author Manuscript

Author Manuscript

Author Manuscript

Table 2.

Absolute maximum difference and RMS of the residuals obtained when comparing the values for $\bar{y}_F$ and $\bar{y}_D$ coming from experimental measurements with the microdosimeter, G4-DNA simulations (with cylindrical site) and analytical calculation (for spherical site). Maximum residuals are also provided in relative value respect to the second set of data, which are shown by absolute differences, enclosed by brackets.

		Maximum (keV/μm)	RMS (keV/μm)
$\bar{y}_F$	Simulation - Experimental	−0.64 (−1.03%)	0.47
	Analytical - Simulation	−0.38 (−0.31%)	0.26
	Analytical - Experimental	−1.01 (−1.29%)	0.71
$\bar{y}_D$	Simulation - Experimental	0.89 (1.17%)	0.61
	Analytical - Simulation	−0.79 (−2.18%)	0.44
	Analytical - Experimental	−1.39 (−3.33%)	0.98